Proceedings of the International Gas Turbine Congress 2003 Tokyo
November 2-7, 2003

IGTC2003Tokyo TS-118

Mechanical Properties and Castability of a 4th Generation Ni-base Single Crystal Superalloy TMS-138

Yasuhiro AOKI[1], Mikiya ARAI[1], Kazuyoshi CHIKUGO[2]
Yutaka KOIZUMI[3], and Hiroshi HARADA[3]

[1] Ishikawajima-Harima Heavy Industries Co., Ltd., Aero-Engine & Space Operations
3-5-1 Mukoudai-cho, Nishi-tokyo-city, Tokyo 188-8555, JAPAN
Phone: +81-424-60-1202, FAX: +81-424-60-1197, E-mail: yasuhiro_aoki_1@ihi.co.jp
[2] Ishikawajima-Harima Heavy Industries Co., Ltd., Research Laboratory
[3]National Institute for Materials Science

ABSTRACT

In order to improve thermal efficiency of jet engines and to reduce the fuel consumption, research and development have been made to apply high performance Ni-base single crystal (SC) superalloys to high-pressure turbine (HPT) blades. TMS-138 alloy, which was developed by National Institute for Materials Science (NIMS) and IHI in the research of High Temperature Material 21 Project, is one of the promising alloys for the future jet engine application.

In this research, creep rupture, high cycle fatigue (HCF), and low cycle fatigue (LCF) tests were performed for several TMS alloys (TMS-75, 82+, 121, and 138 alloys) and CMSX-4 to evaluate the potential of these alloys. TMS-138 alloy showed superior mechanical properties to other alloys. Moreover, TMS-138 alloy showed good oxidation resistance by applying aluminide diffusion coating. Castability was demonstrated by casting the model HPT blades and succeeded.

1. INTRODUCTION

In order to improve thermal efficiency of aero-engines and to reduce the fuel consumption, the cooling air reduction of high-pressure turbine (HPT) blades is required (one of the solution). For this purpose, Ni-base single crystal (SC) superalloys have been applied to increase metal temperature of the HPT blades for modern jet engine. Ni-base SC superalloys have higher performance (especially, creep strength) compared to conventional and directionally solidified superalloys.

Ni-base SC superalloy in the early stage of practical use that is called the 1st generation SC superalloy does not contain Rhenium (Re), for example, Rene'N4 (Ross et at., 1995) and CMSX-2 (Harris and Erickson, 1979). After that, the 2nd generation SC superalloy contains about 3% Re was developed to improve the creep strength. The 2nd generation SC superalloys ,for example, PWA1484 (Cetel and Duhl, 1988), Rene'N5 (Wukusick and Buchakjian, 1991) and CMSX-4 (Harris and Erickson, 1987) have already applied to turbine blades of engines. Moreover, recently, the 3rd generation SC superalloys containing higher Re than the 2nd generation alloys are developed and start using in the engine, for example, CMSX-10 (Erickson, 1994). In Japan, National Institute for Materials Science (NIMS) takes the lead to designs high performance SC superalloys. TMS-138 alloy, which was developed by NIMS and IHI in the research of High Temperature Material 21 Project (Koizumi et al., 2001, J. X. Zhang et al., 2002),contains not only Re but also Ruthenium (Ru) to improve alloy stability. This alloy is designed to have a large negative γ/γ' lattice misfit to improve creep strength and have the attractive potential as next generation SC superalloy.

In this research, in order to evaluate the applicability of TMS-138 alloy to HPT blades, material properties were evaluated by comparing with other SC alloys. Also, to understand the manufacturability of this alloy, some studies of heat treatment and casting process for the HPT blades were conducted.

2. MECHANICAL PROPERTIES OF TMS-138 ALLOY

2.1. Experimental procedure

TMS-138, TMS-75, which was developed by NIMS (Kobayashi et al., 1997), TMS-82+, which was developed by NIMS and Toshiba (Hino et al., 2000), TMS-121 which was developed by NIMS and IHI, and CMSX-4 were used for this research. Chemical compositions of TMS-alloys and CMSX-4 are shown in Table 1.

The alloys cast into cylindrical specimens and had been arranged so that the longitudinal direction became parallel to the crystal growth direction (001). The size of the specimens is ϕ13 x 170mm. After casing, the specimens were heat-treated with the conditions optimized from a microstructural viewpoint during solution and two steps of aging. Creep rupture, high cycle fatigue (HCF), and low cycle fatigue (LCF) tests were performed for the alloys.

2.2. Results and discussion

The creep rupture strength of alloys plotted against Larson-Miller parameter is shown in Fig.1. Creep temperature capabilities of TMS alloys based to that of CMSX-4 at 1000 hours under 137MPa are shown in Fig. 2. TMS-138 alloy is mostly superior to the other alloys. Microstructures after creep rupture tests are shown in Fig.3. No TCP (Topologically Close Packed) phase is observed in TMS-82+ alloy. On the other hands, precipitation of TCP is observed in TMS-121 alloy. Creep strength

Table 1 Chemical compositions of TMS alloys and CMSX-4 (wt%)

	Al	Ti	Ta	Mo	W	Re	Hf	Cr	Co	Ru	Ni
TMS75	6.0	—	6.0	2.0	6.0	5.0	0.1	3.0	12.0	—	Bal.
TMS82+	5.3	0.5	6.0	1.9	8.7	2.4	0.1	4.9	7.8	—	Bal.
TMS121	6.0	—	6.0	3.0	6.0	5.0	0.1	3.0	6.0	—	Bal.
TMS138	5.8	—	5.6	2.9	6.2	5.2	0.1	2.8	5.9	1.9	Bal.
CMSX-4	5.6	1.0	6.5	0.6	6.0	3.0	—	6.5	9.0	—	Bal.

Manuscript Received on August 6, 2003

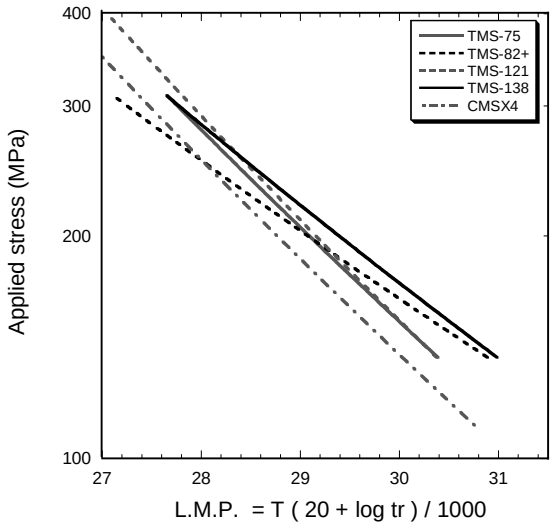

Fig. 1 Creep rupture properties of TMS alloys and CMSX-4.

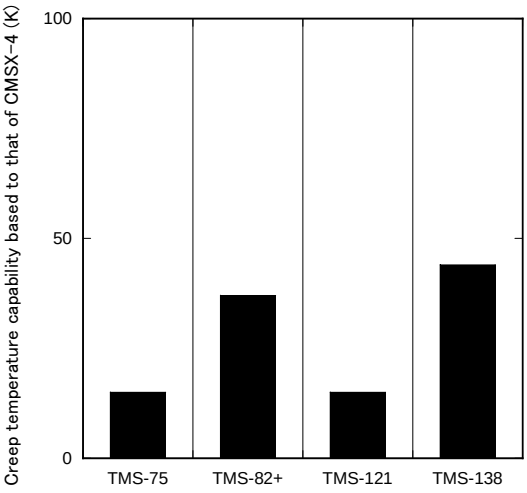

Fig. 2 Creep temperature capabilities of TMS alloys based to that of CMSX-4 at 1000Hr under 137MPa.

decreases as the amount of TCP phase increases as shown in this result. Although Re addition contributes generally to solid solution strengthening, if excess amount of Re addition, the microstructural stability reduce, that is, TCP phase precipitates in the initial stage of creep. Accordingly, SC superalloy to which the amount of Re is only changed, that is 3rd generation SC superalloys and TMS-121 alloy, had a limit of improvement in creep strength, maintaining microstructural stability. Although TCP phase is also observed in TMS-138 alloy, the amount of the phase is less than that in TMS-121 alloy. TMS-138 alloy contains same level of Re to TMS-121 alloy but also 2% of Ru. The chemical compositions of TMS-138 alloy seem to be effective to optimize negative γ/γ' lattice misfit, to improve microstructural stability and to control precipitation of TCP phase. Therefore, TMS-138 alloy had excellent creep strength relative to other alloys.

HCF and LCF failure stress of TMS alloys and CMSX-4 are shown in Fig. 4. The failure stresses were arranged the ratio in comparison with CMSX-4 with each number of failure cycles. As for TMS-138 alloy, HCF failure stress at 1373K and LCF failure stress at 1073K are mostly superior to any alloy.

From these results, it is said that TMS-138 alloy showed most excellent performance relative to other alloys.

(a) TMS-82+

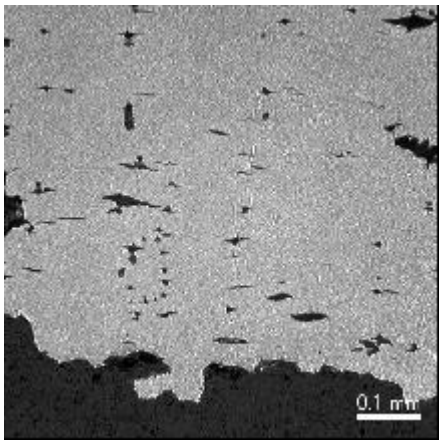

(b) TMS-121

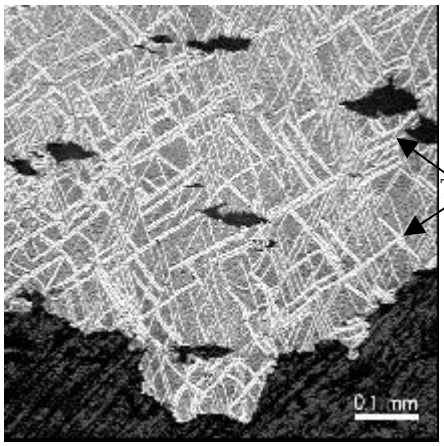

(c) TMS-138

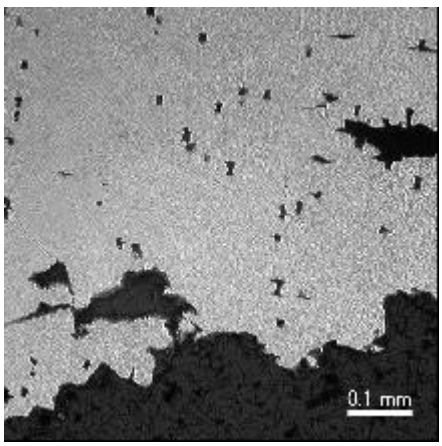

Fig. 3 Microstructure observations at center after creep rupture tests about the alloys.

3. ENVIRONMENTAL RESISTANCE TMS-138 ALLOY

3.1. Experimental procedure

TMS-138 alloy of ϕ20 x 3mm disks was prepared. After solution heat treatment, half of them were applied aluminide

(a) HCF failure stress ratio at 1373K; R ratio:1.0.

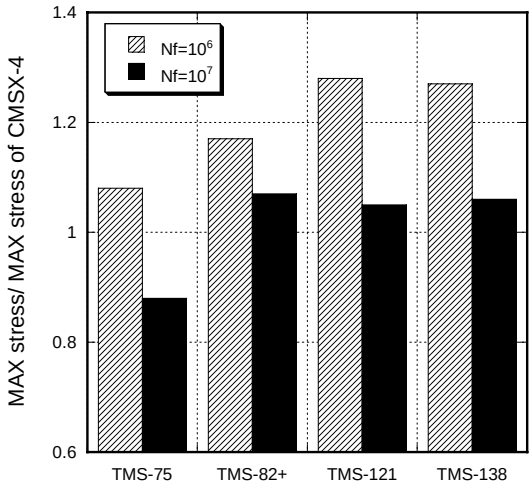

(b) LCF failure stress ratio at 1073K; A-ratio: 1.0.

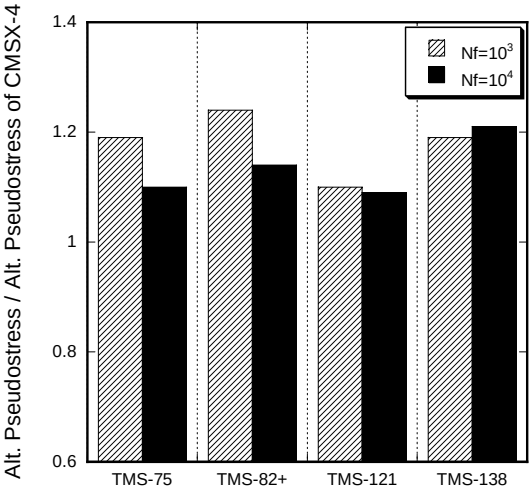

Fig. 4 HCF and LCF failure stress ratio of TMS alloys and CMSX-4.

diffusion coating (CODEP coating). Left of half was tested without coating (bare material). Static oxidation test was carried out with the condition of 1373K in 500 hours air. The weight change of the disk during the tests was measured.

3.2. Results and discussion

The weight changes of TMS-138 alloy during static oxidation test of with and without coating are shown in Fig. 5. The result of CMSX-4 without coating is also plotted in Fig. 5 to compare. Until 100 hours, weight change of TMS-138 alloy is equivalent to that of CMSX-4. However, exceeding 100 hours, TMS-138 alloy shows poor oxidation resistance than CMSX-4. From this result, oxidation resistance coating is essential to use TMS-138 alloy for long term survive. By applying the aluminide diffusion coating, the oxidation resistance is dramatically improved and the weight change is within the limits of ±1 mg/cm^2 even after 500 hours.

The microstructures of both before test and after test for TMS-138 alloy with aluminide diffusion coating are shown in Fig. 6. SRZ (Secondary Reaction Zone) is observed after tests below the coating diffusion layer. As SRZ is said to decrease the creep rupture property (Walston et al., 1996), it might be necessary to develop the

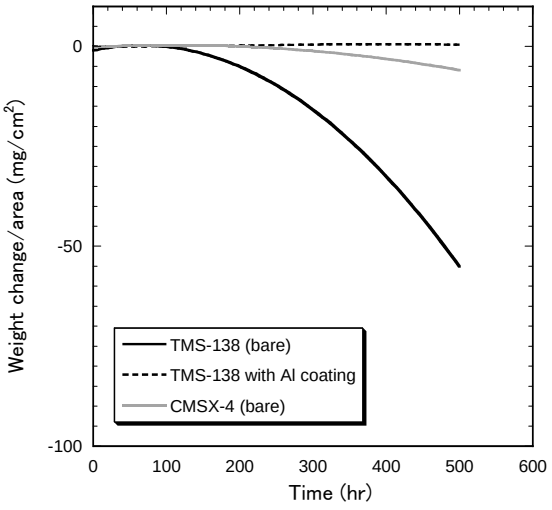

Fig. 5 Static oxidation tests of both bare alloys and Al coated TMS-138 alloy at 1373 in air.

(a) before oxidation test

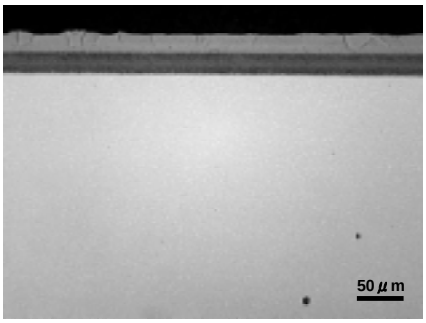

(b) 1373K×500Hr

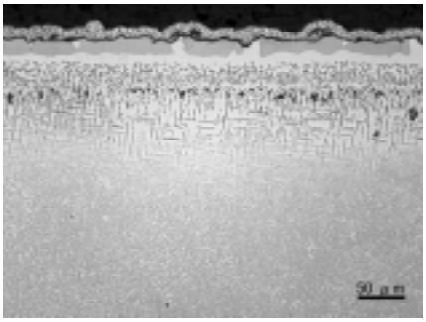

Fig. 6 Microstructures of TMS-138 alloys with Al coating before and after oxidation test.

alternate coating to control the growth of SRZ.

4. HEAT TREATMENT AND CASTING PROCESS STUDY

Generally, HPT blade with complex cooling system has different thickness at dovetail and at airfoil. The difference of thickness might affect the properties because the cooling rates after solution heat treatment is different depending on the thickness. It should be important to understand the effect of cooling rate and cast thickness on mechanical properties.

Moreover, castability should be understood in order to get in service the HPT blade using new alloy.

(a) Position of Specimens

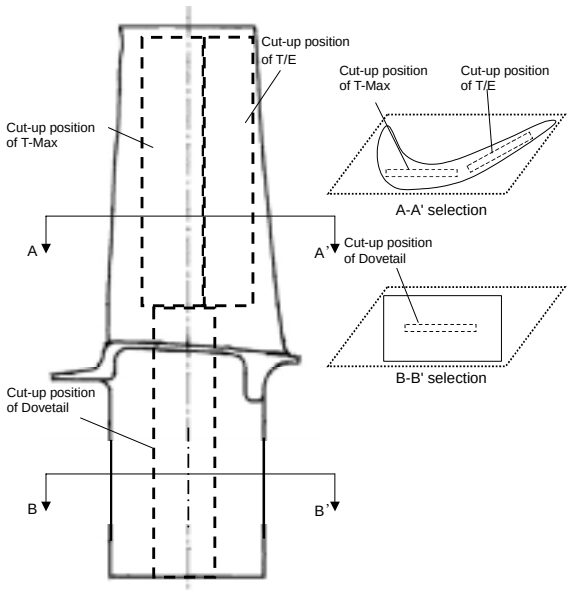

(b) Creep rupture specimen

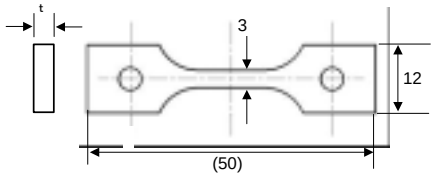

Fig. 7 Specimen shape cutting from model blades and the position machined specimens out.

4.1. Experimental procedure

4.1.1. Cooling rate study

Cast bar of ϕ13 x 170mm were heat-treated with four different cooling methods (oil quench, air cool, gas fan cool and furnace cool) after solution heat treatment. After primary and secondary aging, creep rupture tests were conducted at 1373K under 137MPa.

4.1.2. Cast test of HPT blade

HPT blades were cast using TMS-138 alloy. HPT blade at first stage of HYPR (Hypersonic Transport Propulsion System (Watanabe, 1994)) was selected as the model blade. This blade is about 100mm height and have complex cooling hollows. Fluorescent penetrant inspection (FPI), X ray inspection and grain inspection were carried out after casting. Some of blades were cast without ceramic core and resulted in the blades without cooling hollows. These solid blades were used for the creep test cut from the blade. The position machined the specimens out is shown in Fig 7.

4.2. Results and discussion

4.2.1. Creep rupture strength and microstructure of different cooling method

The microstructures after each heat treatment is shown in Fig. 8, and the relation between cooling rate and γ' phase average size is shown in Fig. 9. The γ' phase size decreases as cooling rate increases, and is proportional to the logarithm of cooling rate. The results of both CMSX-4 for Blum et al. (1994) evaluation and TMS-82+ alloy for the authors (Aoki et al., 2002) are also plotted in Fig. 9. These alloys show indicates the same relations as the TMS-138 alloy. Therefore, it can be said that TMS-138 alloy has the same cooling rate sensitivity to other SC alloys

The relation between cooling rate and creep rupture strength is shown in Fig. 10. Although creep rupture life increased as cooling rate increased when cooling rate is slower than 5K/sec, the life decreased as cooling rate above 5 K/sec. It becomes clear from the creep rupture strength changes according to cooling rate, and

(a) Oil quench; O.Q.

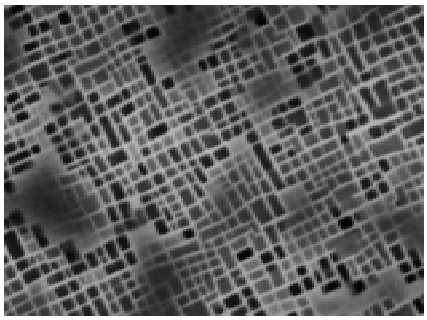

(b) Air cool; A.C.

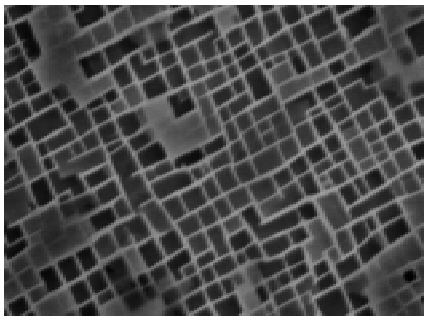

(c) Gas fan cool; G.F.C

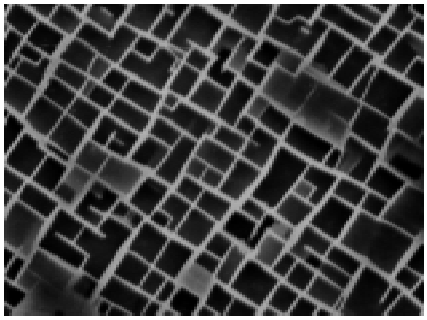

(d) Furnace cool; F.C.

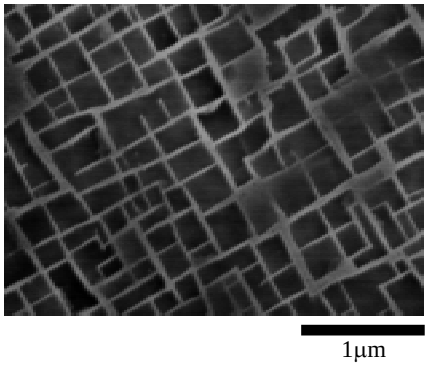

Fig. 8 SEM images after each heat treatment.

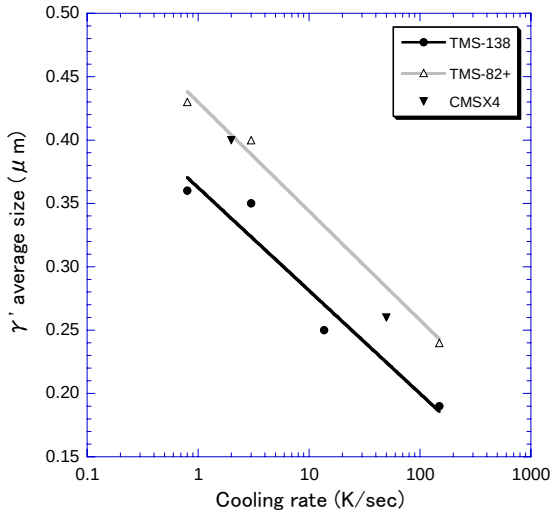

Fig. 9 Relation between cooling rate and γ' phase average size.

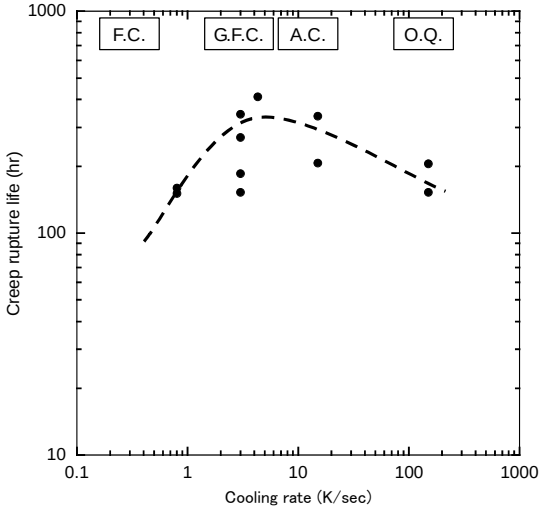

Fig. 10 Relation between cooling rate and creep rupture strength at 1373K under 137MPa.

about 5 K/sec is the optimal cooling rate in TMS-138 alloy.

4.2.2 Cast test of HPT blade

An typical example of HPT balde appearance is shown in Fig. 11. The harmful cast defects, such as shrinkage, inclusion and recrystalized grain were not observed by means of the non-destructive evaluations. The cross-sectional microstructure of the cast blade is shown in Fig. 12. The size of γ' phase observed in each part of blades is the almost same.

Creep rupture strength of specimens cut from blades is shown in Fig. 13. As comparison, the result of cylindrical specimens in the section 2 is also shown in Fig. 13 No significant difference is observed between cut up position and cylindrical specimens. Therefore, it can be clear that the cooling rate, microstructure, and creep rupture strength do not change within the blade used in this study.

5. SUMMARY

1. Creep rupture, high cycle fatigue (HCF), and low cycle fatigue (LCF) tests were performed for TMS alloys, (TMS-75, 82+, 121, and 138 alloys) and CMSX-4. TMS-138 alloy showed most excellent performance relative to other alloys.

Fig. 11 Typical HPT balde of TMS-138 alloy.

2. TMS-138 alloy showed good oxidation resistance by applying aluminide diffusion coating

3. It becomes clear from the creep rupture strength changes according to cooling rate, and about 5 K/sec is the optimal cooling rate in TMS-138 alloy.

4. The harmful cast defects, such as shrinkage, inclusion and recrystalized grain were not observed by means of the non-destructive evaluations.

5. It can be clear that the cooling rate, microstructure, and creep rupture strength do not change within the blade used in this study.

ACKNOWLEDGEMENT

The authors would like to express their thanks to the New Energy and Industrial Technology Development Organization (NEDO) and the Ministry of Economy, Trade and Industry (METI), who gave them the opportunity to conduct "Research and Development of Environmentally Compatible Propulsion System for Next-Generation Supersonic Transport (ESPR) project"

REFERENCES

E. W. Ross, C. S. Wukusick and W. T. King, 1995, "Nickel-Based Superalloys For Producing Singe Crystal Articles Having Improved Tolerance To Low Angle Boundaries", U. S. Patent 5399313.

K. Harris and G. L. Erickson, 1979, "Single crystal (single grain) alloy", U. S. Patent 4582548.

D. N. Duhl and A. D. Cetel, 1988, "Advanced High Strength Single Crystal Superalloy Compositions", U. S. Patent 4719080.

C. S. Wukusick and L. Buchakjian, 1991, "Improved Property Balanced Nickel-base Superalloys for Producing Single Crystal Articles", U. K. Patent Appl. GB2235697.

K. Harris and G. L. Erickson, 1987, "Single Crystal Alloy Technology", U. S. Patent 4643782.

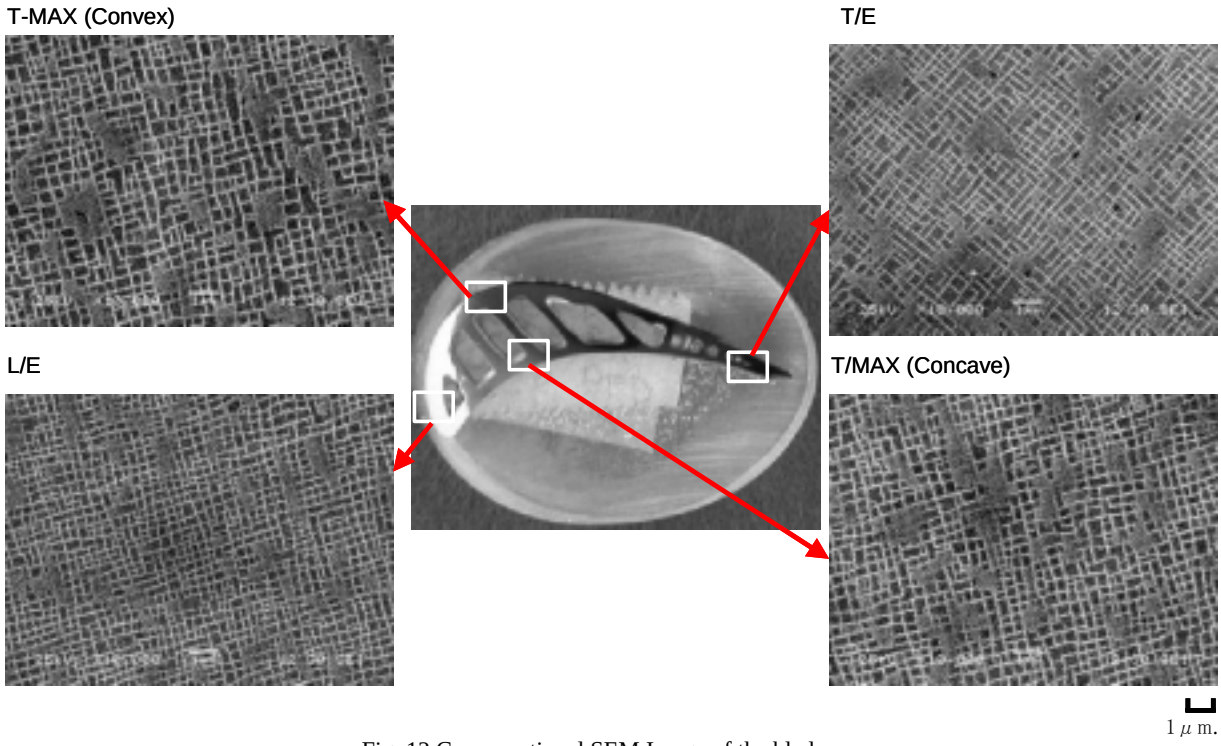

Fig. 12 Cross-sectional SEM Image of the blades.

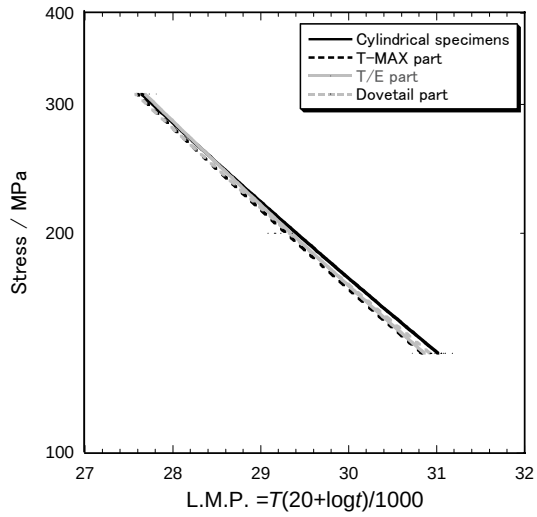

Fig. 13 Creep rupture strength of several part specimens for TMS-138 alloy

G. L. Erickson, 1994, "Single crystal nickel-based superalloy", U. S. Patent 5366695.

Y. Koizumi et al., 2001, "Development of 4th Generation Ni-base Single Crystal Superalloys", presented at 2nd Intern. Sympo., High Temperature Materials 2001, pp.30-31.

J. X. Zhang et al., 2002, "Interfacial Dislocation Networks Strengthening a Fourth-Generation Single-Crystal TMS-138 Superalloy", Metal. and Mat. Trans. A, Vol.33A pp.3741-3746.

T. Kobayashi et al., 1997, "Design of High Rhenium Containing Single Crystal Superalloys with Balanced Intermediate and High Temperature Creep Strengths", Advances in Turbine Materials, Design and Manufacturing, pp.766-773.

T. Hino et al., 2000, "Development of a Single Crystal Superalloy for Industrial Gas Turbines", SUPERALLOY 2000, pp.729-736.

W. S. Walston et al., 1996, ""A New Type of Microstructural Instability in Superalloys-SRZ", SUPERALLOY 1996, pp.9-18.

Y. Watanabe et al., 1994, "Research and Development of Turbo Engine in HYPR Project", Ishikawajima-Harima Engineering Review, Vol.34 No.3 pp.161-171.

F. Blum et al., 1994, "The Effect of Cooling Rate on the γ' Size in Single Crystal Nickel-Base Superalloys", J. Mat. Sci. Let. Vol. 13 pp.1213-1214.

Y. Aoki et al., 2002, "Development of High Temperature Single Crystal Superalloys -High Temperature Material 21 Projects- ", Ishikawajima-Harima Engineering Review, Vol.42 No.4 pp.232- 237.